Electromechanical Energy Conversion Systems (EECS)
Niroo Research Institute (NRI)
Vol. 5, No. 1, Winter 2026, pp. 1-7
DOI: 10.30503/eecs.2025.517409.1073
Original Article

Design of Axial Field Switched Reluctance Motor for Light Vehicle Applications

Alireza Sohrabzadeh[1], Solmaz Kahourzade[2], Amin Mahmoudi[3], Hossein Torkaman[1*]

Abstract

This paper presents the design and analysis of an axial flux switched reluctance motor (AFSRM) developed as a propulsion system for electric vehicle applications. The proposed motor leverages an axial flux topology to achieve high torque density and compact construction. Detailed electromagnetic modeling through the finite element method (FEM) was conducted to evaluate its performance, including flux density, phase current, induced voltage, flux linkage, electromagnetic torque, and torque ripple characteristics. Results indicate that the AFSRM delivers superior performance in terms of operational reliability, making it an attractive solution for modern and light electric drive systems with low speed and high torque density. This paper also discusses the motor's suitability for lightweight and high-efficiency applications, highlighting its potential for future advancements in sustainable transportation.

Keywords: Axial flux machine, switched reluctance motor, finite element method, electric transportation.

Received Date:2025-04-17; Revised Date:2025-05-25; Accepted Date:2025-12-27

I. INTRODUCTION

Switched reluctance motors (SRMs) have emerged as a compelling choice in modern electric motor applications due to their simple construction, high reliability, and cost-effectiveness [1, 2]. Operating on the variable reluctance principle, SRMs achieve torque generation through the alignment of the rotor with the path of minimum reluctance under the influence of a magnetic field created by stator windings [3]. This operational mechanism ensures robustness and high torque density, making SRMs well-suited for various industrial and transportation applications where performance and durability are paramount [4]. The absence of permanent magnets can be considered a crucial advantage of SRMs, especially in cost-effective designs under various conditions [5].

Among the diverse configurations of SRMs, axial field switched reluctance motors offer significant advantages over their radial counterparts [6]. The axial configuration inherently provides a compact design, higher torque density, and superior power-to-weight ratio, which are critical in applications constrained by space and efficiency requirements [7]. These attributes make AFSRMs particularly attractive for mobility solutions such as electric wheelchairs and Scooters, where compactness, efficiency, and reliability are essential for user comfort and safety [8]. However, the design and operation of AFSRMs pose unique challenges, including intricate electromagnetic interactions, elevated noise and vibration levels, and the need for advanced control strategies to ensure optimal performance [9].

While SRMs have been widely researched, several issues limit their broader adoption. High torque ripples, pronounced acoustic noise, and low power factors are among the most significant drawbacks [10]. These issues are particularly critical in axial configurations due to their unique structural and operational characteristics [11]. Addressing these challenges is vital for light vehicle applications, where smooth and precise torque delivery is crucial for maneuverability and user experience [12].

The current body of literature highlights extensive efforts to overcome these challenges in SRMs [13]. Research has focused on improving performance through innovative rotor and stator designs, advanced material applications, and noise and vibration reduction techniques [14]. Although AFSRMs have been explored for specific applications, their application in personal mobility devices remains underdeveloped [15].

Most studies have primarily addressed radial configurations, leaving a critical gap in the understanding and development of axial designs tailored for low-speed and high-torque transportation solutions [16, 17].

[1] *Faculty of Electrical Engineering, Shahid Beheshti University, Tehran, Iran.*
[2] *STEM, University of South, Australia, Adelaide, Australia.*
[3] *College of Science and Engineering, Flinders University, Adelaide, Australia.*
**Corresponding author, Email: h_torkaman@sbu.ac.ir*

Light vehicles such as electric wheelchairs demand motors capable of delivering consistent torque at low speeds to ensure smooth movement, stability, and the ability to handle inclines or uneven terrains [18, 19]. Traditional DC motors dominate this domain due to their ease of control and adequate performance. However, their efficiency and reliability often lag behind reluctance-based motors [20]. Integrating the benefits of SRMs into electric vehicles presents a significant opportunity to enhance energy efficiency, reduce maintenance, and improve overall user satisfaction [21, 22]. The unique challenges associated with torque ripple, noise, and precise control in axial configurations must be addressed to unlock their full potential in this domain.

The growing demand for compact, energy-efficient, and reliable motors for personal mobility underscores the importance of developing axial SRMs optimized for electric vehicles. In general, the axial configuration's compactness and superior torque characteristics align well with the requirements of modern mobility solutions [23]. Overcoming the associated design and operational challenges can lead to the creation of a transformative motor solution, bridging the gap between efficiency, reliability, and user-centric performance. A successful design of an AFSRM for electric wheelchairs has the potential to revolutionize mobility technology, offering a cost-effective and high-performance alternative to conventional motor solutions.

This study aims to address these critical challenges by designing an axial field switched reluctance motor for electric wheelchair applications. By focusing on the electromagnetic and control aspects, the proposed motor seeks to harness the inherent advantages of SRMs while meeting the stringent performance and reliability standards required for personal mobility devices. The outcomes of this research will provide valuable insights into the development of next-generation motor technologies that combine efficiency, robustness, and user comfort.

This paper is arranged in four distinct sections. First, in section II, a general statement about operation as well as design procedure is presented. Then, as an essential step in Section III, electromagnetic performance is assessed, involving two different driving conditions. In section IV, a short statement of the author's outlook is stated, and section V identifies salient achievements.

II. THE ESSENCE OF OPERATION

In this section, after a brief review of the principles of operation, the desired topology is designed, and the method of study is discussed.

A. The nature of AFSRM Operation

The main concept of the design of AFSRMs has been intensively discussed in [22, 23], and in this paper, the same strategy for the design procedure was used.

In general, in AFSRMs, torque is generated through the interaction between the stator and rotor magnetic fields, and the torque ripple depends on the variation of the inductance with rotor position. Below are the key equations that describe the operation of the AFSRMs, along with the formula for torque ripple.

The electromagnetic torque in an SRM is given by the rate of change of the magnetic energy stored in the motor's inductance concerning the rotor position (θ) [24]:

$$T = \sum_{i=1}^{m} \left(\frac{1}{2} .I^2 . \frac{dL(\theta,I)}{d\theta} \right)_m \quad (1)$$

where I, and $L_s(\theta,I,)$ represent the phase current and self-inductance, respectively, and m refers to several phases.

Also, torque ripple in AFSRMs occurs due to the periodic variation in the inductance as the rotor moves. The torque ripple factor can be expressed as [25]:

$$T_{ripple}(\%) = \frac{(\text{Maximum torque}) - (\text{Minimum torque})}{(\text{Average Torque})} \times 100 \quad (2)$$

The torque ripple is directly related to the variation in the inductance, and more specifically, to the shape of the inductance concerning rotor position.

The smoother the inductance profile, the lower the torque ripple. Conversely, sharp variations in the inductance lead to higher torque ripple, which is undesirable as it can cause vibration and reduce the motor's efficiency. The inductance profile is usually approximated as a sinusoidal or piecewise linear function, but in practice, the inductance curve may have sharp transitions that cause higher torque ripple [24].

B. Design of 12/16 AFSRM

Axial Flux Switched Reluctance Motor with 16 rotor poles was designed and employed a single-stator topology as illustrated in Fig.1.

AFSRMs that feature fewer pole counts have larger pole arcs and hence lower switching frequency. They simplify manufacturing, reduce core losses, and enhance efficiency at lower operating speeds. Conversely, topologies with higher rotor poles, like 16-pole AFSRM, leverage a higher pole count to achieve smoother torque output and reduced ripple. The smaller pole pitch in this configuration necessitates higher switching frequencies and more precise control strategies, increasing its complexity but enabling superior dynamic performance. However, due to the desired applications, a combination of 3-phase SRM with 12 poles in the stator as well as 16 poles in the rotor was selected.

Noteworthy that a uniform excitation pattern of the coil was used, such that coils of the same phase were excited oppositely next to each other [25].

Table I provides detailed design parameters. In addition, the B-H curve of the steel used for the stator and rotor is indicated in Fig.2.

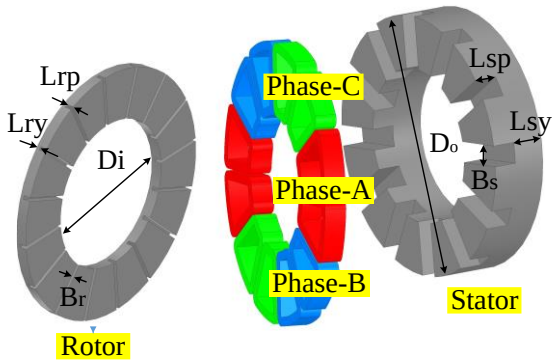

Fig. 1. Exploded view of the designed AFSRM.

TABLE 1. Key Parameters of the Designed AFSRM.

Parameter	Value
Pole Numbers (Ps / Pr)	12/16
Stator and Rotor materials	M 19-24G
Winding Material	Copper
Outer Diameter (D_o)	275 mm
The ratio of D_O/ D_i	0.59
Inner Diameter (D_i)	163 mm
End-winding	15 mm
Air-Gap (g)	0.5 mm
Stator yoke length (L_{sy})	35 mm
Stator pole length (L_{sp})	25.5 mm
Rotor yoke length (L_{ry})	4 mm
Rotor pole length (L_{rp})	8.5 mm
Stator slot width (B_s)	22 mm
Rotor slot width (B_r)	4 mm
Current density (J)	4 A/mm^2
DC Voltage (V_{dc})	590 V
Rated torque (T)	28 Nm
Rated Speed (ω)	750 rpm
Number of phases (m)	3
Number of turns per phase (N_{ph})	180
Slot fill factor	0.45
Resistance per phase (Rs)	0.26 Ω
Inductance per phase (Ls)	2.5 mH

To drive a designed motor, both voltage and current excitation types are examined in this paper. As shown in Fig. 3,(a), an asymmetric bridge drive circuit is used for voltage excitation, and pulse sources are also used to drive the motor. The nature of the voltage mode excitation will be based on the operation of the switches, which will turn on 7.5 degrees of each phase for a period of 22.5 degrees of switching.

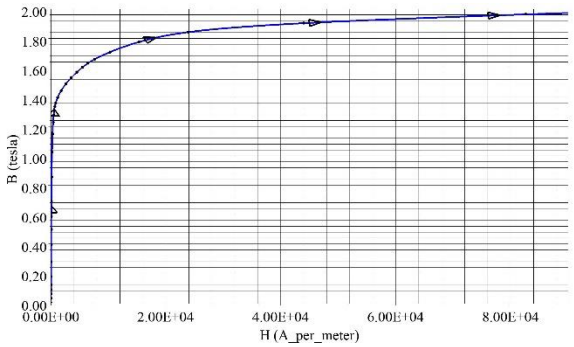

Fig. 2. B-H curve of used steel.

The same strategy will be applied to the current-driven mode as depicted in Fig.3 (b), where a delay equal to 7.5 degrees should be considered between each phase and pulse generator, with an amount of 10A used to excite different phases respectively. Noteworthy that Fig.3 reports ideal circuits without the values of winding resistance and inductance that have been reported in Table 1.

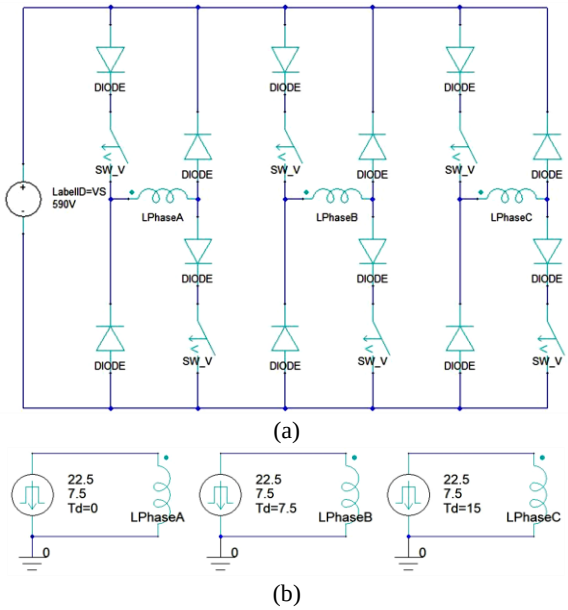

(a)

(b)

Fig. 3. Ideal circuit of: (a) Voltage drive (Asymmetric Bridge Converter) with two switches and four diodes in each phase, and (c) Current drive with current pulse sources.

III. ELECTROMAGNETIC EVALUATION

In this section, motor performance is examined in two voltage and current modes.

A. Voltage-Driven Mode

Fig. 4 shows the flux density for the entire structure and for the rotor in both the fully unaligned and aligned positions.

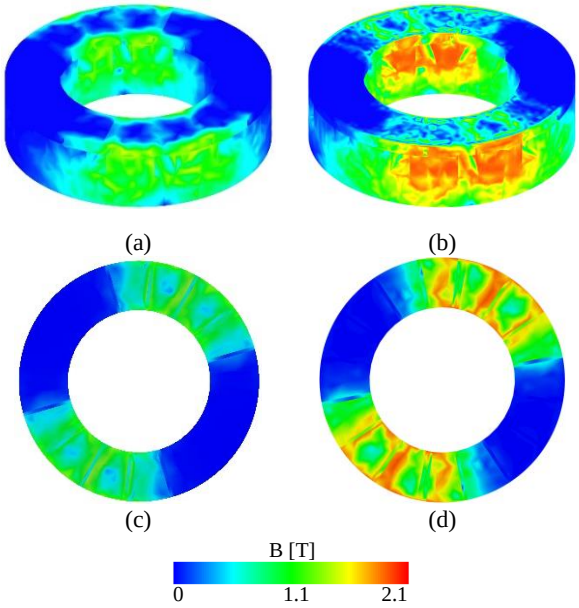

Fig. 4. (a) Flux density of the entire structure of 12/16 AFSRM at (a) unaligned position, (b) aligned position; and front surface of rotor of 12/16 AFSRM at (c) unaligned position, (d) aligned position.

In the unaligned position, the maximum flux density in the designed model is recorded at 1.2 Tesla, where the maximum flux linkage is seen in the aligned state at the excited phase. As it is clear, due to the type of excitation pattern that is placed next to each other, about a third of the structure is in the maximum flux state, while in the vicinity of it, leakage fluxes will occur in the other phases.
In the maximum magnetic reconnection excitation state, it helps to produce more torque in the AFSRM, considering the magnetization curve of the material.

Fig. 5 demonstrates the phase currents for the designed structure. In a period of 22.5 degrees, each phase will be conducted for 7.5 degrees. Under voltage conditions, a constant speed interval of about 0.75 is considered as the commutation area for activating each switch to avoid sudden changes due to current changes and torque drops. The maximum phase current for each phase is 30 (A).

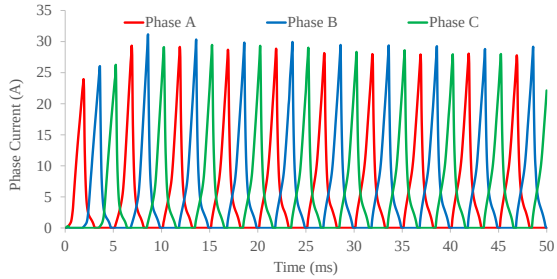

Fig. 5. Phase Currents of the designed 12/16 AFSRM at 750 rpm in voltage-driven mode.

In addition, shown in Fig. 6 is the amount of voltage that is applied to the phases after switching. As it is clear, the switching behavior is visible in both current and voltage forms to the same extent, and also, the maximum voltage of 590 has been measured on each winding. The reverse voltage applied to the winding is to drain and return the current to the source through the diodes.

In Fig.7, the flux linkage for all three phases is shown. The voltage-type nature of the excitation will create a transient condition that is about. 10 to 20 ms for the designed structure. The symmetry in the measured flux value indicates the correct switching operation.

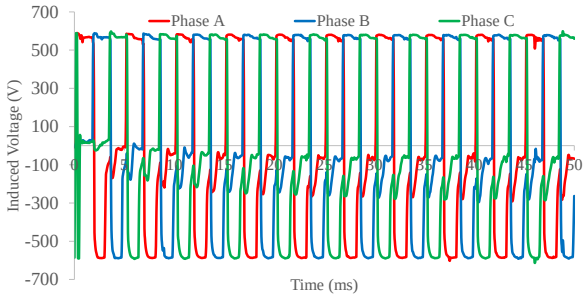

Fig. 6. Induced Voltages of the designed 12/16 AFSRM at 750 rpm voltage-driven mode.

The dynamic torque profile is shown in Fig. 8. The transient behavior of this type of excitation is visible. After reaching a steady state, which is considered to be about 35 ms, the average torque value reaches 29.45 Nm. Under this condition, the torque ripple value is measured to be 49%.

To calculate efficiency, the following equation is used[15]:

$$\eta\,(\%)=\frac{P_{output}}{P_{in\text{-}ph}}\times 100 \qquad (3)$$

$$P_{output}=T.\omega\ ;$$

$$P_{in\text{-}ph}=\sum_{i=1}^{m} v_{ph}\times i_{ph}\ ;$$

where v_{ph} and i_{ph} are the voltage and current of the phase, respectively.

The numerical results are detailed in Table II. It is noteworthy that all reported features are calculated under voltage-driven conditions.

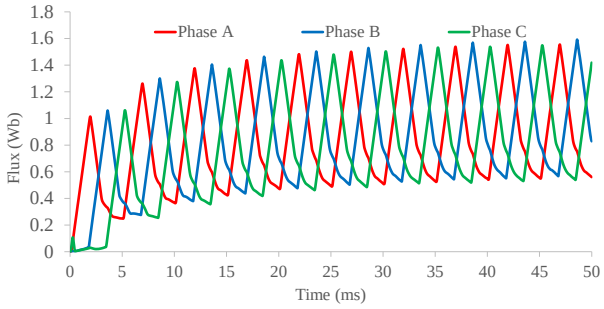

Fig. 7. Flux linkages of the designed 12/16 AFSRM at 750 rpm in voltage-driven mode.

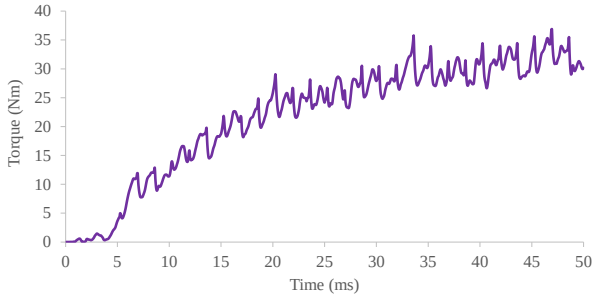

Fig. 8. Dynamic torque profile of the designed 12/16 AFSRM at 750 rpm in voltage-driven mode.

B. Current-Driven Mode

In this section, torque and flux profiles are shown under current excitation conditions.

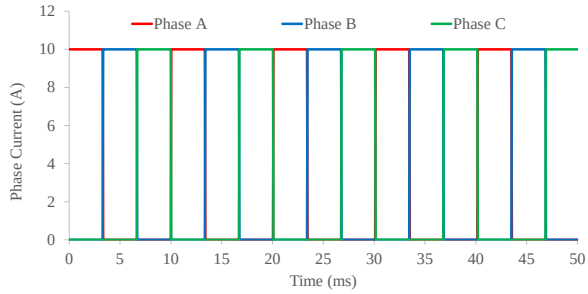

Fig. 9. Phase currents of the designed 12/16 AFSRM at 750 rpm in current-driven mode.

The sample current of 10 A is chosen regarding the RMS value of current, which is achieved by the voltage-driven mode in the previous section. However, to provide a different operating condition of the structure, the current-driven mode is studied apart from the voltage-driven mode. The current profiles of different phases in the current mode are shown in Fig.9.

Initially, the flux linkage is given in Fig. 10. As stated in Table II, its maximum value is about 1.10 Wb. It has created a relatively different profile compared to the voltage excitation condition, although a relatively similar rise timing can be observed in the transient condition.

The difference in flux linkage profiles between voltage and current excitation stems from the dynamic and nonlinear characteristics of the SRM.

When voltage is applied to the winding, current gradually increases, following Faraday's law [24]:

$$V = \frac{d\lambda}{dt} = Ri \quad (4)$$

Here, the rate of change of flux linkage depends on current growth and winding resistance. Since current varies dynamically, saturation effects and transient delays influence the flux profile.

On the other hand, with direct current control, flux linkage can be explicitly regulated. In this case, inductance significantly influences the flux behavior. Because the current remains controlled, nonlinear effects (such as saturation) impact the flux profile less [26]:

$$\lambda = L(i, \theta).\, i \quad (5)$$

Hence, voltage excitation leads to rapid current growth, causing saturation and altering the flux rate. In addition, voltage control introduces transient behavior in flux linkage due to variable inductance. While in the current excitation, a better control minimizes unexpected flux variations.

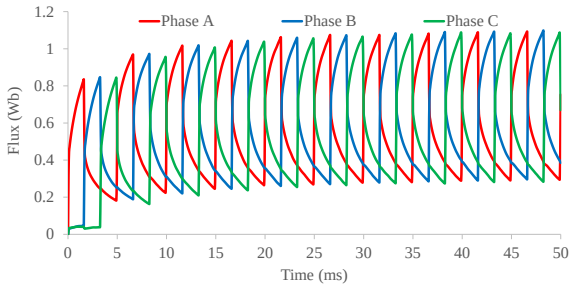

Fig. 10. 3-Phase flux linkage of the 12/16 AFSRM in current-driven mode at 10 A.

The torque study for the condition where a current of 10 A is applied to the coils is given in Fig. 11. For the conditions where the torque profile reached its steady state, that is, after 30 ms, the average torque value registered 13.5 Nm, and the torque ripple recorded 40.79 %.

It is an acceptable criticism that any electric motor with this percentage of torque ripple is not suitable for transportation. However, the target of this paper was only the primary step of the design of AFSRM regarding required dimensions and boundaries, as well as the dynamic evaluation of performance. Yet, further work in this area to tackle this unwanted issue will be publicized according to this simple design in the future.

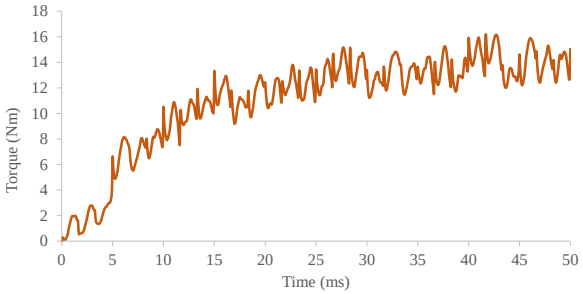

Fig. 11. Dynamic torque profile of the 12/16 AFSRM in current-driven mode at 10 A.

To conclude, the numerical results validate that AFSRMs offer a compelling alternative to conventional motor types in light electric vehicle systems, not only by meeting performance benchmarks but also by addressing cost-effectiveness and sustainability goals. With its scalability and adaptability, the proposed motor design holds the potential to drive advancements in eco-friendly transportation where permanent magnets are not used, offering a viable solution to modern mobility challenges.

TABLE 2. Performance Parameters of the Designed 12/16 AFSRM

Item	12/16 AFSRM
Voltage-Driven Mode	
Average Torque (Nm)	29.45
Excited Voltage (V)	590
Speed	750 rpm
Torque Ripple (%)	49
Maximum Phase Current (A)	30.2
RMS Phase Current (A)	9.57
Maximum Flux Linkage (Wb)	1.59
Efficiency (%)	96
Current-Driven Mode	
Excited Current (A)	10
Maximum Flux Linkage (Wb)	1.10
Average Torque (Nm)	13.5
Torque ripple (%)	40.79

IV. Future Works

What was stated in this article involves the numerical design and simulations of an axial field switched reluctance motor for light vehicle applications such as wheelchairs and scooters. Generally, the percentage of torque ripple in the SRMs is a preventive factor to realize them in the form of electric transportation. In this way, supplementary methods, both in terms of structural and control aspects, are required to solve these tricky issues. Thus, the primary steps of a completed design will be associated with torque ripple reduction techniques. While the optimization steps, comparison with other types of structures, as well as designs from other perspectives, such as mechanical and thermal, can be carried out, which will be derived from the designed model shortly. In addition, the discussion of the construction of the intended applicability will be more reliable, which is the goal of studies shortly.

V. Conclusion

This study presented the design and analysis of an axial field switched reluctance motor tailored for light electric vehicle applications. The motor's unique axial flux topology, combined with its inherent advantages such as high torque density, mechanical robustness, and simple construction, makes it an ideal candidate for light transportation applications like wheelchairs and scooters. To verify the effectiveness of the designed topology, more than one excitation condition and setting parameters were simulated. The results were coherent compared to the numerical design. The proposed topology is recorded 29.45 Nm at 750 rpm in Voltage-Driven condition as well as 13.5 Nm at 10 A in Current current-driven condition, both with a torque ripple factor of about 40%. Through detailed electromagnetic and performance evaluations, the proposed design demonstrated its applicability, aligning with the critical requirements of light vehicles, including lightweight construction and high reliability.

References

[1] A. Sohrabzadeh, H. Torkaman, and A. Y. Javid, "Improvement Undesirable Characteristics of the Switched Reluctance Motor with Triangular Rotor Structure," *IEEE Transactions on Energy Conversion*, pp. 1-8, 2023.

[2] E Afjei, H Torkaman, "Airgap eccentricity fault diagnosis in switched reluctance motor," *1st Power Electronic & Drive Systems & Technologies Conference*, Tehran, Iran, 2010, pp. 290-294.

[3] H. Torkaman and A. Sohrabzadeh, "Reduction of inappropriate principal features of the switched reluctance motor using sinusoidal rotor configuration," *IET Electric Power Applications*, vol. n/a, no. n/a, 2023.

[4] H. Torkaman, A. Ghaheri, and A. Keyhani, "Axial flux switched reluctance machines: a comprehensive review of design and topologies," *IET Electric Power Applications*, vol. 13, no. 3, pp. 310-321, 2019.

[5] A. Y. Javid, A. Sohrabzadeh, H. Torkaman, S. Kahourzade, A. Mahmoudi, and W. L. Soong, "Switched Reluctance Motor with Permanent-Magnet Embedded Rotor Ring for Torque Enhancement in High Speed Applications," in *2024 6th International Conference on Smart Power & Internet Energy Systems (SPIES)*, 2024, pp. 53-57.

[6] R. Madhavan and B. G. Fernandes, "A novel axial flux segmented SRM for electric vehicle application," in *The XIX International Conference on Electrical Machines - ICEM 2010*, 2010, pp. 1-6.

[7] R. Madhavan and B. G. Fernandes, "Performance Improvement in the Axial Flux-Segmented Rotor-Switched Reluctance Motor," *IEEE Transactions on Energy Conversion*, vol. 29, no. 3, pp. 641-651, 2014.

[8] Z. Cao, A. Mahmoudi, S. Kahourzade, and W. L. Soong, "An Overview of Electric Motors for Electric Vehicles," in *2021 31st Australasian Universities Power Engineering Conference (AUPEC)*, 2021, pp. 1-6.

[9] A. Sohrabzadeh and H. Torkaman, "W-shaped Rotor Switched Reluctance Motor for Magnetic Forces Enhancement: Design, Analysis, and Comparative Study," in *2023 3rd International Conference on Electrical Machines and Drives (ICEMD)*, 2023, pp. 1-6.

[10] A. Y. Javid, A. Sohrabzadeh, H. Torkaman, S. Kahourzade, A. Mahmoudi, and W. L. Soong, "A Novel Switched Reluctance Motor with Semi-Hard Material in Rotor for High-Speed Applications," in *2024 IEEE Energy Conversion Congress and Exposition (ECCE)*, 2024, pp. 5735-5741.

[11] M. H. Belhadi, G. Krebs, C. Marchand, H. Hannoun, and X. Mininger, "Evaluation of axial SRM for electric vehicle application," *Electric Power Systems Research*, vol. 148, pp. 155-161, 2017/07/01/ 2017.

[12] P. Azer, B. Bilgin, and A. Emadi, "Comprehensive Analysis and Optimized Control of Torque Ripple and Power Factor in a Three-Phase Mutually Coupled Switched Reluctance Motor With Sinusoidal Current Excitation," *IEEE Transactions on Power Electronics*, vol. 36, no. 6, pp. 7150-7164, 2021.

[13] A. Y. Javid, A. Sohrabzadeh, and H. Torkaman, "Low-Cost Semi-Hard Material in High-Speed 6/2 Switched Reluctance Motor for Eliminating Torque Dead-Zone and Torque Enhancement," in *2024 4th International Conference on Electrical Machines and Drives (ICEMD)*, 2024, pp. 1-6.

[14] C. Gan, J. Wu, Q. Sun, W. Kong, H. Li, and Y. Hu, "A Review on Machine Topologies and Control Techniques for Low-Noise Switched Reluctance Motors in Electric Vehicle Applications," *IEEE Access*, vol. 6, pp. 31430-31443, 2018.

[15] M. A. J. Kondelaji and M. Mirsalim, "Segmented-Rotor Modular Switched Reluctance Motor With High Torque and Low Torque Ripple," *IEEE Transactions on Transportation Electrification*, vol. 6, pp. 62-72, 2020.

[16] S. Kahourzade, A. Mahmoudi, H. W. Ping, and M. N. Uddin, "A Comprehensive Review of Axial-Flux Permanent-Magnet Machines," *Canadian Journal of Electrical and Computer Engineering*, vol. 37, no. 1, pp. 19-33, 2014.

[17] K. Diao, X. Sun, G. Lei, Y. Guo, and J. Zhu, "Multimode Optimization of Switched Reluctance Machines in Hybrid Electric Vehicles," *IEEE Transactions on Energy Conversion*, vol. 36, no. 3, pp. 2217-2226, 2021.

[18] G. Wang, Y. Wang, Y. Gao, W. Hua, Q. Ni, and H. Zhang, "Thermal Model Approach to the YASA Machine for In-Wheel Traction Applications," *Energies*, vol. 15, no. 15, p. 5431, 2022.

[19] S. Dey, B. G. Fernandes, and K. Chatterjee, "A High Torque Density Magnetic Geared Switched Reluctance Motor for In-wheel Applications," in *2024 IEEE Transportation Electrification Conference and Expo (ITEC)*, 2024, pp. 1-6.

[20] F. N. Jurca, R. Mircea, C. Martis, R. Martis, and P. P. Florin, "Synchronous reluctance motors for small electric traction vehicle," in *2014 International Conference and Exposition on Electrical and Power Engineering (EPE)*, 2014, pp. 317-321.

[21] P. Andrada, E. Martínez, B. Blanqué, M. Torrent, J. I. Perat, and J. A. Sánchez, "New axial-flux switched reluctance motor for e-scooter," in *2016 International Conference on Electrical Systems for Aircraft, Railway, Ship Propulsion and Road Vehicles & International Transportation Electrification Conference (ESARS-ITEC)*, 2016, pp. 1-6.

[22] A. Sohrabzadeh, A. Jaferian-Fini, H. Torkaman, and H. Ebrahimi, "Design of PM-Assisted Rotor Alongside Pole Shoes in Reluctance Magnetic Gear for Torque Enhancement," in *2024 4th International Conference on Electrical Machines and Drives (ICEMD)*, 2024, pp. 1-6.

[23] X. Sun, K. Diao, G. Lei, Y. Guo, and J. Zhu, "Study on Segmented-Rotor Switched Reluctance Motors With Different Rotor Pole Numbers for BSG System of Hybrid Electric Vehicles," *IEEE Transactions on Vehicular Technology*, vol. 68, no. 6, pp. 5537-5547, 2019.

[24] R. Krishnan, R. Arumugan, and J. F. Lindsay, "Design procedure for switched-reluctance motors," *IEEE Transactions on Industry Applications*, vol. 24, no. 3, pp. 456-461, 1988.

[25] A. Sohrabzadeh, H. Torkaman, and E. Afjei, "Torque Ripple Reduction and Radial Force Mitigation in the Switched Reluctance Motor Using a Novel Rotor Configuration," in *2023 14th Power Electronics, Drive Systems, and Technologies Conference (PEDSTC)*, 2023, pp. 1-4.

[26] J.-W. Lee, H. Kim, B. Kwon, and B. Kim, "New rotor shape design for minimum torque ripple of SRM using FEM," *Magnetics, IEEE Transactions on*, vol. 40, pp. 754-757, 04/01 2004.